Advanced Composites and Hybrid Materials (2022) 5:1988–2001
https://doi.org/10.1007/s42114-022-00534-y

ORIGINAL RESEARCH

Hybrid biocomposites based on polylactic acid and natural fillers from *Chamaerops humilis* dwarf palm and *Posidonia oceanica* leaves

Roberto Scaffaro[1] · Andrea Maio[1] · Michele Gammino[1]

Received: 30 January 2022 / Revised: 9 May 2022 / Accepted: 14 July 2022 / Published online: 28 July 2022

Abstract

Platelet-like and fibrous lignocellulosic fillers were achieved from the leaves of *Chamaerops humilis* (CHL) and *Posidonia oceanica* (POL) and used as a hybrid reinforcement for a polylactic acid (PLA) matrix at three different loading levels (from 5 to 20%). The materials were fully characterized from a morphological, physicochemical, mechanical, and dynamic-thermomechanical point of view. When compared to their counterpart containing either CHL or POL only, the resulting hybrid biocomposites showed the highest mechanical properties, with strengthening and stiffening effects respectively up to 120% and 50% higher than those expected from the linear combination of the two, and higher dynamic-mechanical performance, with storage moduli in the rubbery region 10 times higher than those of composites containing solely CHL or POL. Such synergistic efficiency is likely due to the formation of a strong and extensive interphase region, promoted by the balanced effect of morphological features of the hybrid network and physicochemical characteristics of the components. These green materials could find applications as panels for furniture or in the automotive industry.

Keywords Hybrid biocomposites · DMA · Dwarf palm · Lignocellulosic fillers · Interphase

1 Introduction

The increasing demand for biodegradable and cost-effective materials stimulated many research efforts towards the design of biocomposites involving natural fillers obtained from widespread and inedible plants, in full compliance with the novel guidelines inspired by circular economy and zero waste [1–3]. While the advantages of natural fillers are undoubted from an economic and ecological point of view, their incorporation into bioplastics often causes a deterioration of the mechanical properties, especially at high loadings [4–8]. Hence, the next challenge in the field of materials science and technology is to replace relatively large quantities of bioplastics with natural fillers in order to design green materials that can combine their well-known cost-effectiveness and renewability with satisfactory mechanical robustness [9–12].

Among the bioplastics, PLA is one of the most promising, owing to its outstanding mechanical performance and biodegradability [13, 14]. Nevertheless, its high production costs currently limit the use of PLA as a commodity [7, 15, 16]. Moreover, when combined with natural fillers, PLA often shows an undesired decay of tensile strength upon filler content [4–7, 17]. On the other hand, hybrid composites containing two or more fillers are gaining a meaningful interest in the perspective of constructing composites having emerging properties exceeding the sum of those of single constituents [18–33]. Indeed, polymeric composites with excellent mechanical performance can be achieved via the integration of a hybrid framework constituted by 1D/2D nanofillers, as in the case of PLA- and polyurethane-based hybrid composites, reinforced with graphene/carbon nanotubes [18, 22, 34–36]. Inspired by this, we designed hybrid biocomposites loaded with natural fibers and platelets obtained from the leaves of inexpensive wild plants, such as *Chamaerops humilis* (also known as Mediterranean dwarf palm) and *Posidonia oceanica*. The selection of these fillers is motivated by some considerations. First, both plants are inedible and largely bio-available. Indeed, their uncontrolled proliferation in the Mediterranean area sometimes forces local authorities to bear additional costs for collecting and disposal [6]. Second, it is possible to attain microparticles with porous architecture and different features, namely platelet-like microparticles from *Posidonia*

✉ Roberto Scaffaro
roberto.scaffaro@unipa.it

[1] Department of Engineering, University of Palermo, Viale delle Scienze, Ed. 6, Palermo 90128, Italy

oceanica leaves (POL) with proven affinity to PLA [5, 37, 38], and cylindrical fibers from *Chamaerops humilis* leaves (CHL). These latter, in particular, were recently tested as reinforcing agents for poly(butylene adipate-co-terephthalate) for the first time [39], showing enormous potential by virtue of their good mechanical resistance coupled with large amounts of lignin that could be advantageous in mitigating the typical thermomechanical degradation that occurs when PLA is processed with lignocellulosic fillers [5, 37, 38].

2 Experimental part

2.1 Materials and processing

Wastes of CHL samples and POL were collected in the western seacoast of Palermo. The two lignocellulosic fillers underwent the same workup protocol, involving thorough washing with water to remove impurities (namely sand, mud, and so on), drying at $T = 120$ °C under atmospheric pressure for a couple of days, and grounding and sieving (70–100 mesh).

PLA (Ingeo 2003D, NatureWorks) used in this work is an extrusion grade having a content of D-lactic acid monomer equal to ~ 4%, $\rho = 1.24$ g/cm^3, MFI = 6 g/10 min, $T_m = 160$ °C, and Mw = 240 kDa. Tetrahydrofuran (THF), reagent grade 99%, was purchased from Sigma-Aldrich.

In order to avoid hydrolytic reactions during processing, all the materials were vacuum-dried overnight at $T = 90$ °C. The schematics of the pathway followed to prepare the biocomposites is provided in Fig. 1.

Twin screw extrusion with a die temperature of 190 °C was used to fabricate neat PLA (as a reference material) and 9 different composite samples, having 5%, 10%, and 20% weight contents of either CHL, POL, or hybrid combination of the two, obtained by adding equal amounts, by weight, of each filler. The material coming from the extruder was continuously pelletized after cooling in water, re-conditioned in vacuum-oven and finally compression molded ($T = 190$ °C, $p = 8$ bar, $t = 2$ min) into prismatic specimens, having width = 10 mm, length = 30 mm, and thickness ~ 0.7 mm.

2.2 Characterizations

Morphology of starting components and biocomposites has been investigated by scanning electron microscopy (SEM) imaging, carried out with a Phenom Pro X instrument (Thermo Fisher Scientific, USA), and optical microscopy (Leica MS5 stereomicroscope). The salient geometrical features of the particles, i.e., length (L), diameter (D), thickness (t), and the resulting aspect ratio (A_f), were

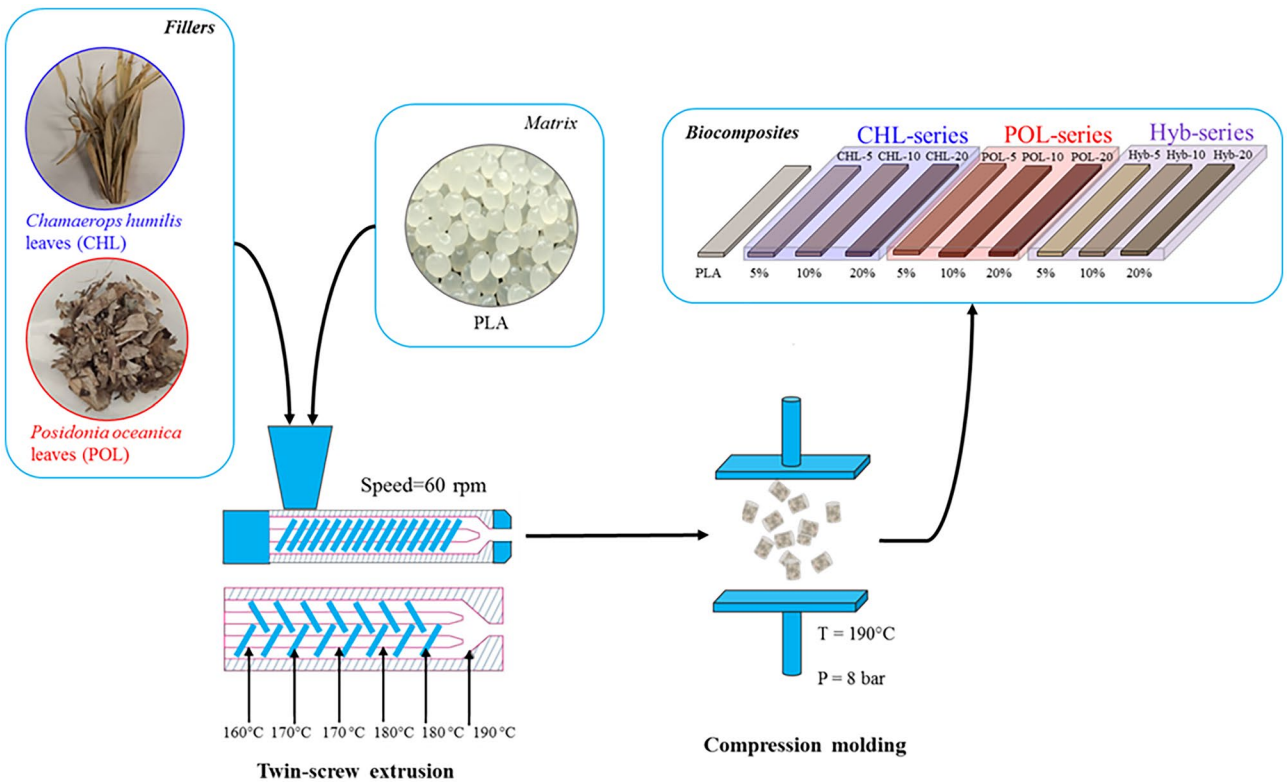

Fig. 1 Schematics of the preparation of green composites

measured by using an open-source, JAVA-based image processing software, ImageJ, onto at least 100 microparticles for each sample. A_f was calculated both before and after processing. In this latter case, the fillers were separated from the matrix by solvent extraction in THF at room temperature. Moreover, this procedure allowed us to evaluate even the effects of processing and fillers on the molecular weight of PLA. In fact, PLA extracted from each composite was dried and then re-dissolved in THF at the concentration of 0.1 wt%. Flow time of each solution was measured by means of iVisc LMV 830 Lauda Proline PV 15 (Lauda-Königshofen, Germany) instrument equipped with a Ubbelohde ($K = 0.009676$) capillary viscometer, and placed in thermostated oil bath at 35 °C. Viscosimetric molecular weight (M_V) of PLA was extrapolated from its intrinsic viscosity by means of the Mark-Houwink constants. More details can be found in our previous studies [38]. M_v values of the polymer processed in the various composites were then normalized to that of unprocessed PLA to obtain an indicator of the chemical state of the matrix in each composite.

Differential scanning calorimetry (DSC) was carried out using a Shimadzu DSC-60. The degree of crystallinity (χ) of PLA in each biocomposite was calculated according to Eq. (1) [40]:

$$\chi = \frac{\Delta H_m - \Delta H_{cc}}{\left(1 - \Phi_w\right)\Delta H_m^0} \tag{1}$$

where ΔH_m and ΔH_{cc} are, respectively, the melting enthalpy and the cold crystallization enthalpy, Φ_w is the filler weight fraction of the given composite, and ΔH_m^0 is the melting enthalpy of 100% crystalline PLA (93.7 J/g [40]).

Density measurements were performed by a Thermo Pycnomatic Helium Pycnometer (Pycnomatic ATC, Thermo Fisher, USA), using a 99.99% pure helium. Measures were repeated at least five times for each sample, at 20 °C. The degree of densification for each material was calculated as the ratio between apparent density and real density. The dispersion degree was measured by analyzing the variance in the composition of each sample, according to the methodology described in the literature [39, 41].

Briefly, the actual degree of dispersion of the filler throughout the polymer matrix was assessed by taking into account the actual filler concentration in a number of randomly chosen samples and compared with the average concentration. Such parameter is given by Eq. (2) [39]:

$$\textit{Dispersion degree} = \left(1 - S/S_0\right) \tag{2}$$

where S is the square root of the variance S^2, defined by Eq. (3) [39] as:

$$S^2 = \frac{1}{N-1}\sum_{i=1}^{N}\left(C_i - \overline{C}\right)^2 \tag{3}$$

where N is the number of samples analyzed, C_i indicates the concentration of the i^{th} sample and $\overline{C}$ is the mean concentration of the N samples. S is normalized to S_0, that is the square root of the maximum variance S_0^2, given by Eq. (4) [39]:

$$S_0^2 = \overline{C}\left(1 - \overline{C}\right) \tag{4}$$

This latter, in fact, is representative of the limit case of a composite in which all the components are completely segregated [42]. The concentration was measured via helium pycnometer on fifty specimens randomly collected from compression-molded sheets.

Tensile tests were carried out by means of an Instron 3365 (Instron, USA) dynamometer, by imposing a crosshead speed of 1 mm/min up to specimen failure, according to ISO 527–3 standard. For each experimental run, at least 10 replicates were tested, and the salient data, namely elastic modulus (E), tensile strength (TS), and elongation at break (EB) were provided as mean values and standard deviations.

Dynamic mechanical properties of the materials were measured using a DMA Metravib 50 (France), in tensile mode. The measurements were carried out at a constant frequency of 1 Hz, a strain amplitude of 0.05%, and in the temperature range 20–70 °C, at a heating rate of 3 °C/min and using a 20-mm gap. Before testing, the samples were dried overnight under vacuum at 90 °C.

3 Results and discussion

Morphometric analysis of CHL and POL, provided in Fig. 2, highlights the different morphology of the fillers, with CHL and POL having fibrous and platelet geometry, respectively. CHL fibers displayed relatively narrow size distributions in terms of both length (average value = 2 mm) and diameter (mean diameter = 150 µm). POL platelets can be regarded as parallelepipeds having constant thickness (25 µm) and variable length and width, with average values respectively equal to 250 µm and 170 µm. Table 1 provides an overview of the salient features of fillers, both showing a porous yet different architecture and similar aspect ratios, but remarkable differences in terms of mechanical performance.

Morphology of biocomposites was assessed by SEM analysis, whose results are shown in Fig. 3. All the samples display not only satisfactory levels of filler dispersion, but also the presence of voids, due to either weak interfacial adhesion, occasionally detected in CHL-series and POL-series composites (at 20%), or empty lumens of fillers. Noteworthy, hybrid composites seem to show denser structure

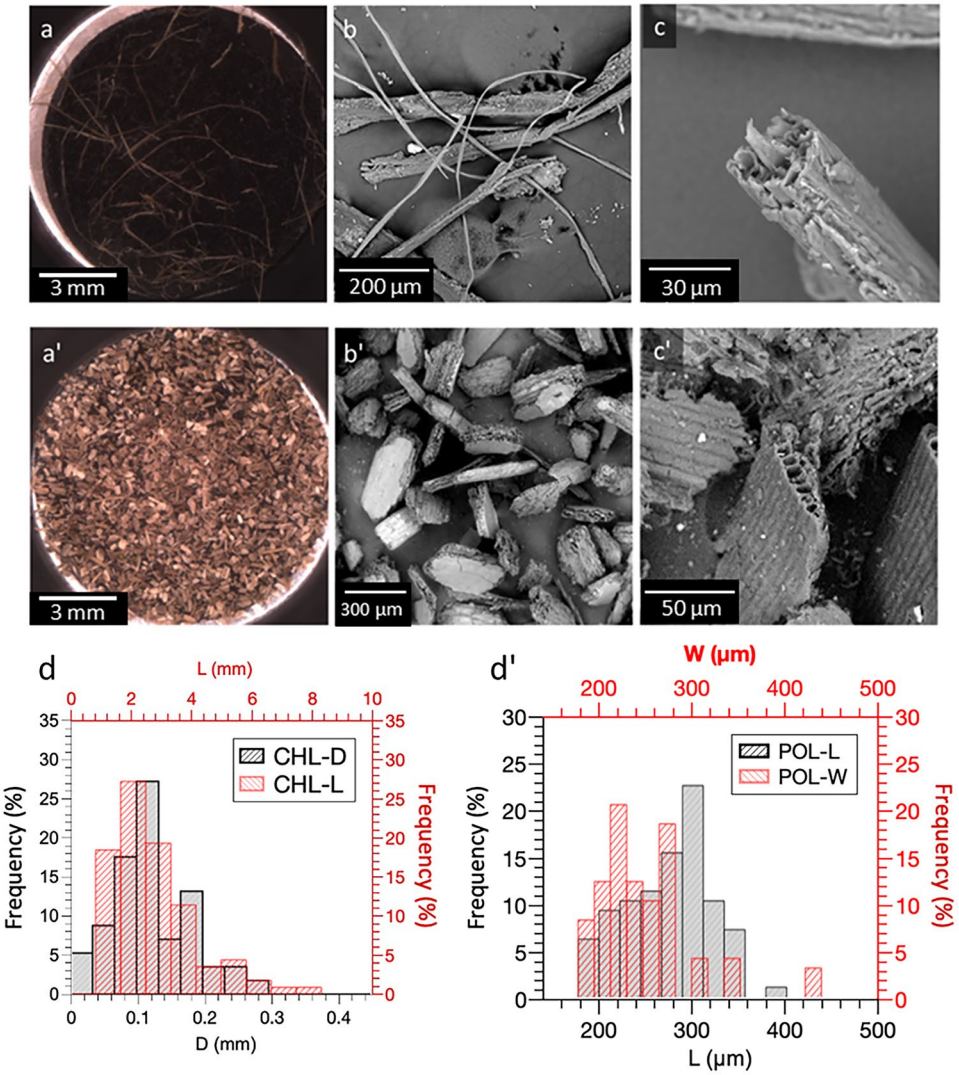

Fig. 2 Morphometric analysis of CHL (top panels) and POL (bottom panels) after grinding and sieving: optical micrographs (**a–a'**), SEM micrographs at different magnifications (**b–c**, **b'–c'**), filler size distributions (**d–d'**)

and stronger filler-matrix adhesion. Morphometric analysis of microparticles after processing was then performed. Figure 4a shows the mapping area of a representative sample (in this case Hyb-20) from which at least 100 particles of each filler were collected for image analysis. As one can see, the processing induced outstanding cleavage events, with all the fillers showing size below millimeter scale.

Table 1 Overview of the salient features of the two fillers

Filler	Mean A_f	Density (g/cm^3)	Porosity (%)	E (GPa)[c]	E_{bulk} (GPa)[d]
CHL	13[a]	1.51	62	4.7	~32
POL	10[b]	1.54	73	0.84	~12

[a]Calculated as L/D

[b]Calculated as D_{eq}/T

[c]Measured by tensile tests on raw fibers

[d]Theoretically calculated (Eq. S1)

As a result, Fig. 4b, A_f of both microparticles has been shown to decrease in all biocomposites, with data scattering higher than the eventual differences among the samples. Figure 4c shows a detailed portion in which it is possible to recognize the size heterogeneity of both CHL, under the form of either fiber bundles or fibrils, and POL platelets. Light-blue and pink arrows respectively indicate the low aspect ratio CHL and POL particles, whereas blue and red arrows highlight those with high aspect ratio. The yellow circle on the right shows a hybrid formed by a fiber protruding from a platelet. It is worth mentioning that residual polymer inclusions were occasionally detected in all the extracted samples, as confirmed by detailed SEM micrographs reported in Fig. 4d and e, respectively, showing CHL and POL particles with totally empty lumens (left panels) or surrounded and interpenetrated by residual PLA (right panels). This latter occurrence is supposed to have positive repercussions on the ultimate properties of the systems.

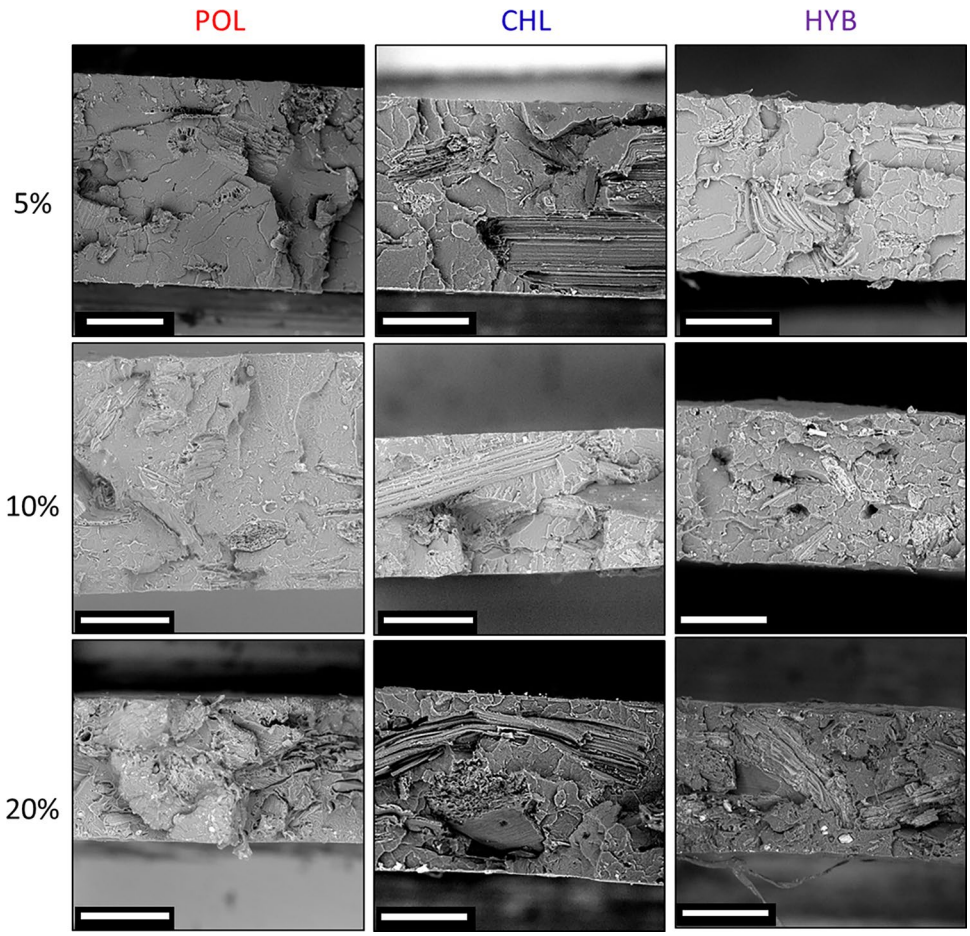

Fig. 3 Cross-sectional SEM micrographs of cryofractured biocomposites

Salient mechanical properties of the samples are reported in Fig. 5. Adding solely CHL or CHS to PLA improved the stiffness with a maximum observed at 10%, while being detrimental to breaking properties, which experienced a monotonic decay. In particular, biocomposites with 20% loading of either CHL or POL display an overall mechanical performance lower than that of neat polymer. In contrast, hybrid biocomposites performed better than CHL- and POL-series materials, resulting in a monotonic increase of both E and TS, at the expense of EB. In order to understand if and when it is advantageous to use hybrid fillers with respect to the single constituents, we constructed a map of synergistic effects on stiffening, strengthening, and stretching at the three different concentrations adopted. The synergetic effect of CHL and POL on the properties of PLA-based composites can be conveniently elucidated by using Eq. (5) [43]:

$$\text{Synergistic efficiency} = \left[2P_{\text{hyb}} - (P_{\text{CHL}} + P_{\text{POL}})\right]/(P_{\text{CHL}} + P_{\text{POL}})] \quad (5)$$

where P_{CHL}, P_{POL}, and P_{hyb} represent the generic property measured for PLA loaded with CHL, POL, and a hybrid combination of CHL and POL, respectively.

In the case of synergy, the synergistic efficiency has positive values (see the green-filled area in the plots), whereas it assumes negative values in the case of destructive interference (red-filled area). Of course, this parameter is equal to 0 in the absence of interactions. As one can see, the simultaneous use of CHL and POL determines a remarkable synergistic efficiency in strengthening in all the concentrations, while having positive repercussions on stiffness only at 20% loading. Furthermore, combining the two fillers proved to be slightly detrimental to deformability, especially at low loadings, differently from what was observed in the case of PLA-based composites containing other lignocellulosic fillers, such as *Opuntia ficus indica* and *Hedysarum coronarium* [4, 17]. Taken together, these data outline that hybrid loading is successful especially at high loading, giving the possibility to prepare materials having 120% and 50% increments of TS and E, while displaying negligible loss of stretchability (−5%) with respect to what would be expected by the linear combination of the behavior of the single fillers. Figure 6 provides a comparison between the elastic moduli experimentally measured and those predicted by Halpin–Tsai model (see SI, Eqs. S2–S6). For this purpose, bulk moduli of fillers were estimated according to Eq.

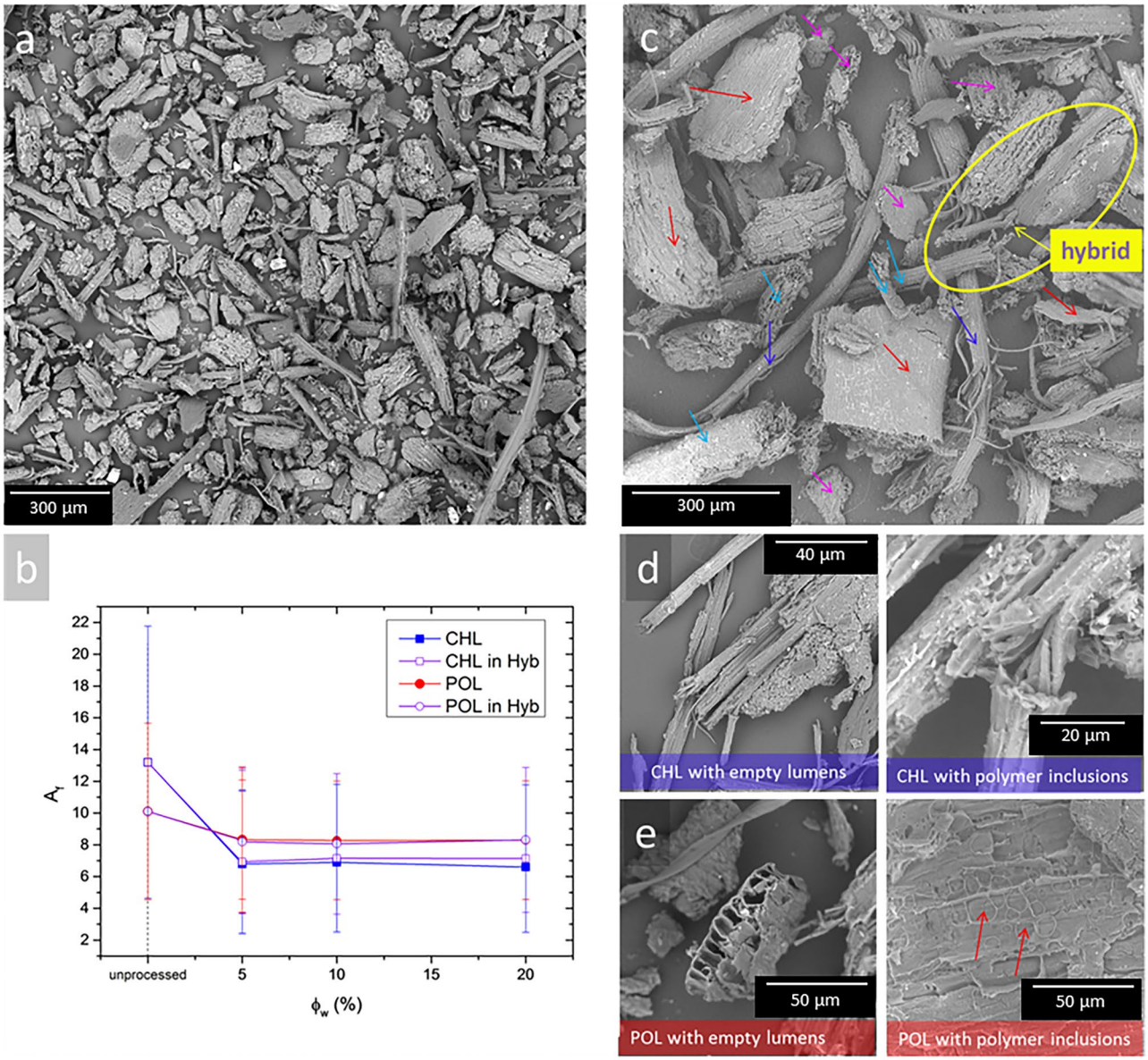

Fig. 4 Mapping area of Hyb-20 (**a**), plots of A_f as a function of filler content and type (**b**); detailed micrograph of Hyb-20 (**c**); detailed micrographs of CHL (**d**) and POL (**e**) particles with empty lumens (left panels) and interpenetrated by residual PLA (right panels)

(S1), while the actual aspect ratio of fillers was measured after solvent extraction of composites, which enabled us to calculate even the polymer molecular weight after processing, useful to monitor the extent of eventual degradation pathways.

The results show that the actual stiffness of all the biocomposites was underestimated at low loadings, and overestimated at the highest content of either CHL or POL, whereas Hyb-20 was satisfactorily fitted. This aspect could likely be explained considering that the polymer inclusions inside the lumens could have led to the formation of an effective reinforcing phase fraction greater than the nominal one, whereas segregation and voids observed at 20% filler content could have reduced the reinforcing phase fraction. Green and red arrows in the plots respectively highlight the positive and negative deviations from the nominal filler fraction according to the H-T model.

Beyond this, the ultimate properties of a composite material may depend on several factors, including physicochemical features of the polymer matrix, such as crystallinity and eventual degradation, and morphological parameters, such as the degrees of densification and filler dispersion/adhesion, with the latter depending on the affinity between components [44, 45]. An overview of these parameters is provided in Fig. 7 for composites containing CHL (a), POL (b), and Hyb (c). CHL-based biocomposites display negligible

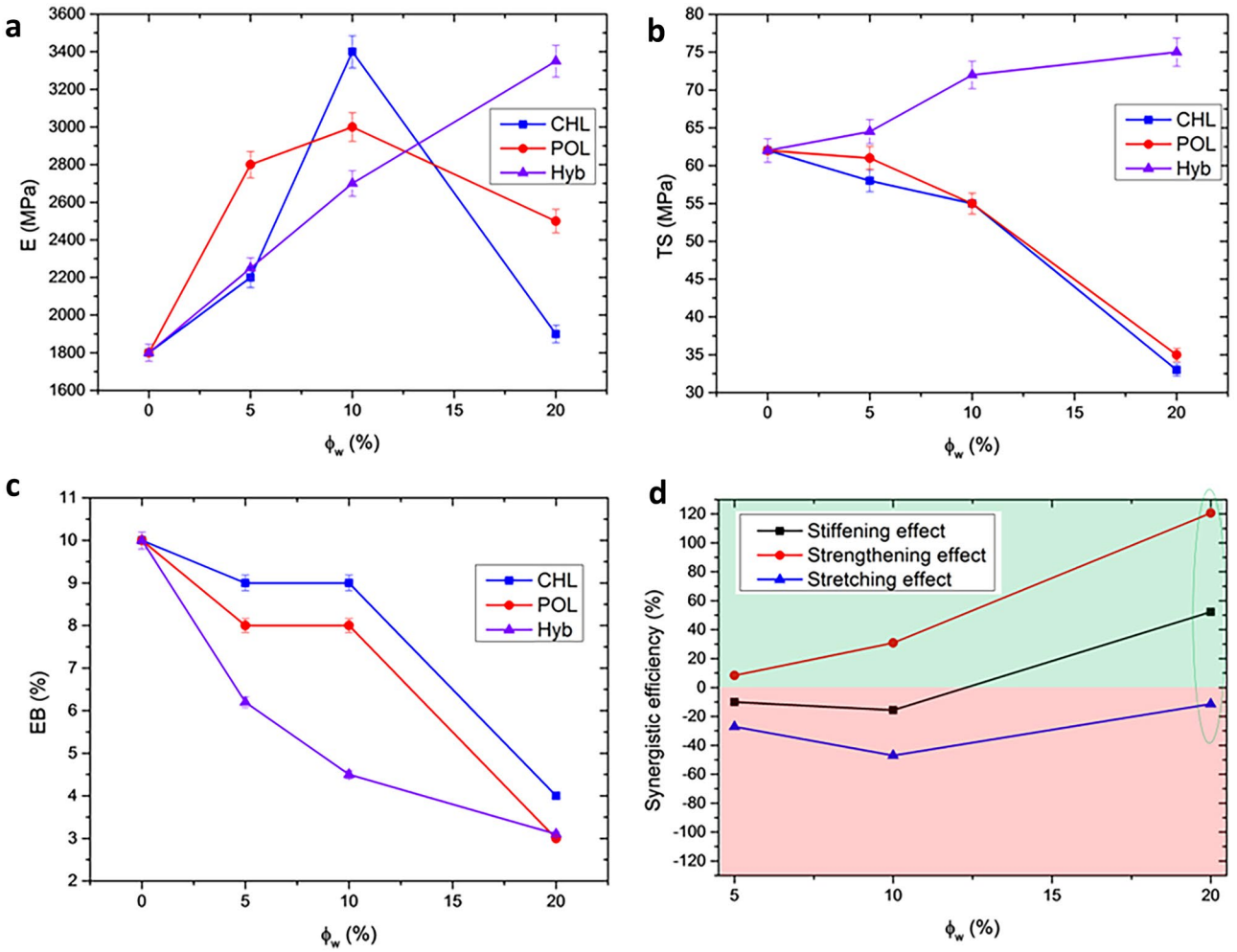

Fig. 5 Behavior of *E* (**a**), TS (**b**), and EB (**c**) as a function of filler content, synergistic efficiency of hybrid fillers in stiffening, strengthening, and stretching (**d**)

degradative phenomena, with the matrix substantially retaining similar molecular weights as that of processed PLA, regardless of filler content. Due to its amorphous nature, PLA showed a low degree of crystallinity, ranging from 1.8 to 6%, with a maximum observed at 10% filler content. Therefore, CHL had negligible effects on the physicochemical characteristics of the matrix, while on the other hand affecting the morphological features of composites in a dose-dependent manner, with optimal values of both densification and dispersion degrees observed at 10% content, in full agreement with the results of mechanical properties. On the contrary, the behavior of morpho-chemical parameters in POL-series materials reflects the complex interactions between POL and PLA, with morphological and physicochemical aspects interrelating each other. POL microparticles exerted the highest pro-degradant activity, with a clear dose-dependent trend. Note that in POL-20 the matrix displays a molecular weight halved compared to the PLA processed in the same way, as already envisaged in previous studies [5, 38]. Consequently, POL samples exhibited the highest crystallinity degrees, even at high filler content, although the maximum was observed at 5% loading. Moreover, the extensive degradation might somehow have contributed to enable the more hydrophilic and shorter polymer chains to interact with the filler, giving rise to an unexpected rise of dispersion index at 20% content. For the same reasons, densification degrees of POL-series samples, yet lower than those of the other composites, proved to be satisfactory, especially considering the outstanding porosity of POL platelets (74%). Hybrid loading led to composites with morphochemical properties scarcely dependent on loading level. Densification and degradation extents proved to be intermediate between those of the two single fillers, while no effect was found on crystallization behavior of PLA, which remained amorphous (see again Fig. S1). Noteworthy, such composites displayed the highest levels of dispersion. This

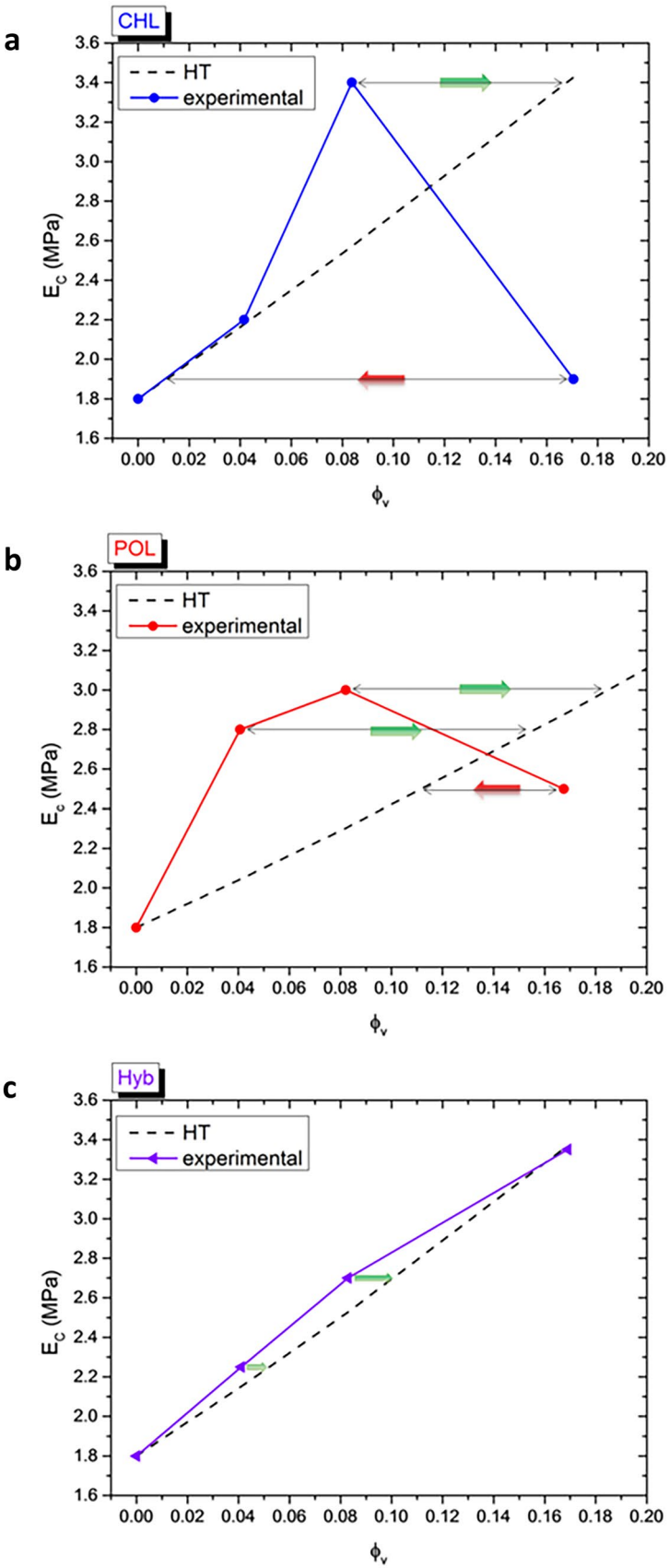

Fig. 6 Comparison between HT predictions and experimental data for CHL (**a**), POL (**b**), and Hyb (**c**) biocomposites

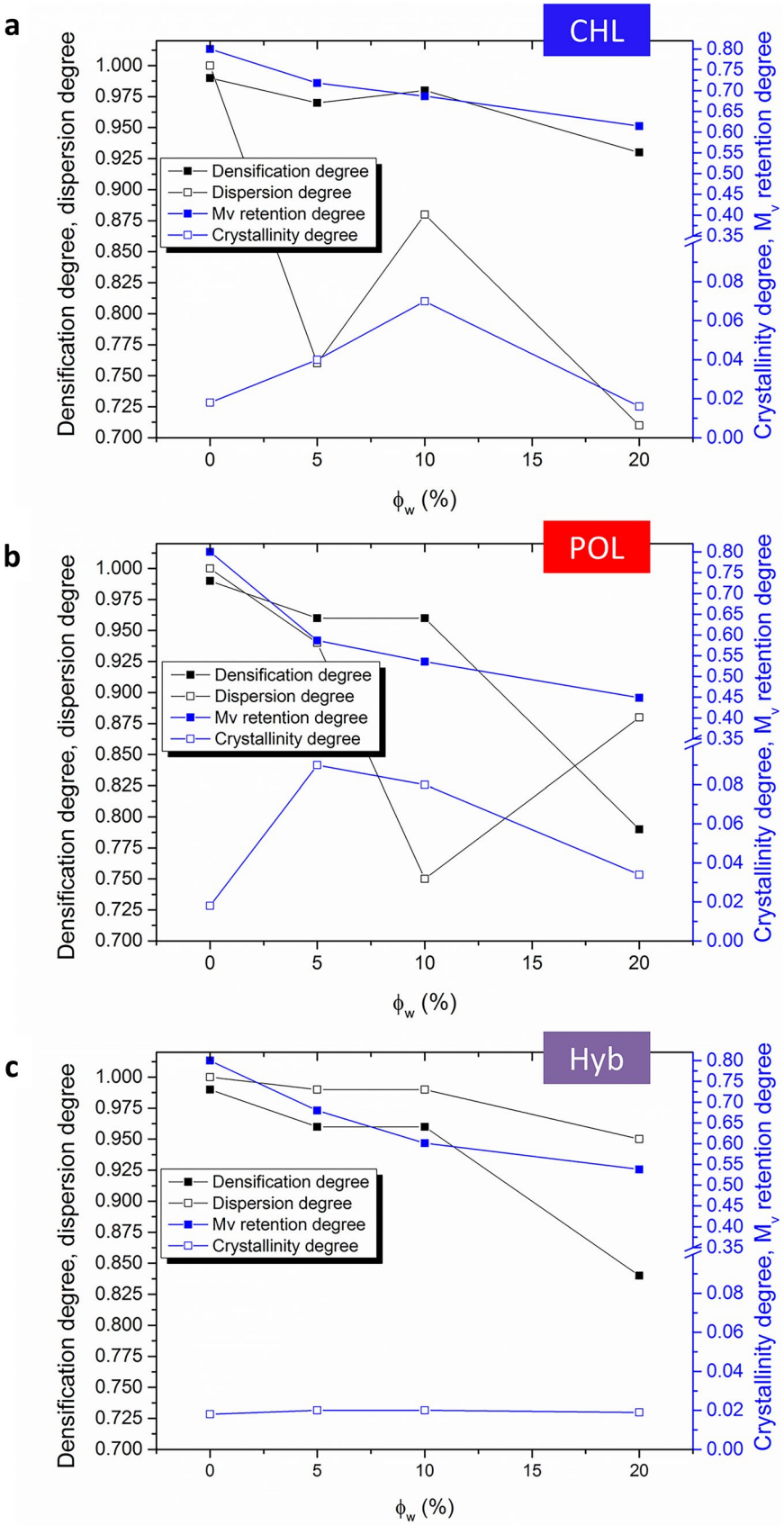

Fig. 7 Overview of morphological properties (densification and dispersion degrees, left axis) and physicochemical features of the matrix (M_v retention and crystallinity degrees, right axis) in CHL- (**a**), POL- (**b**), and Hyb-series materials (**c**)

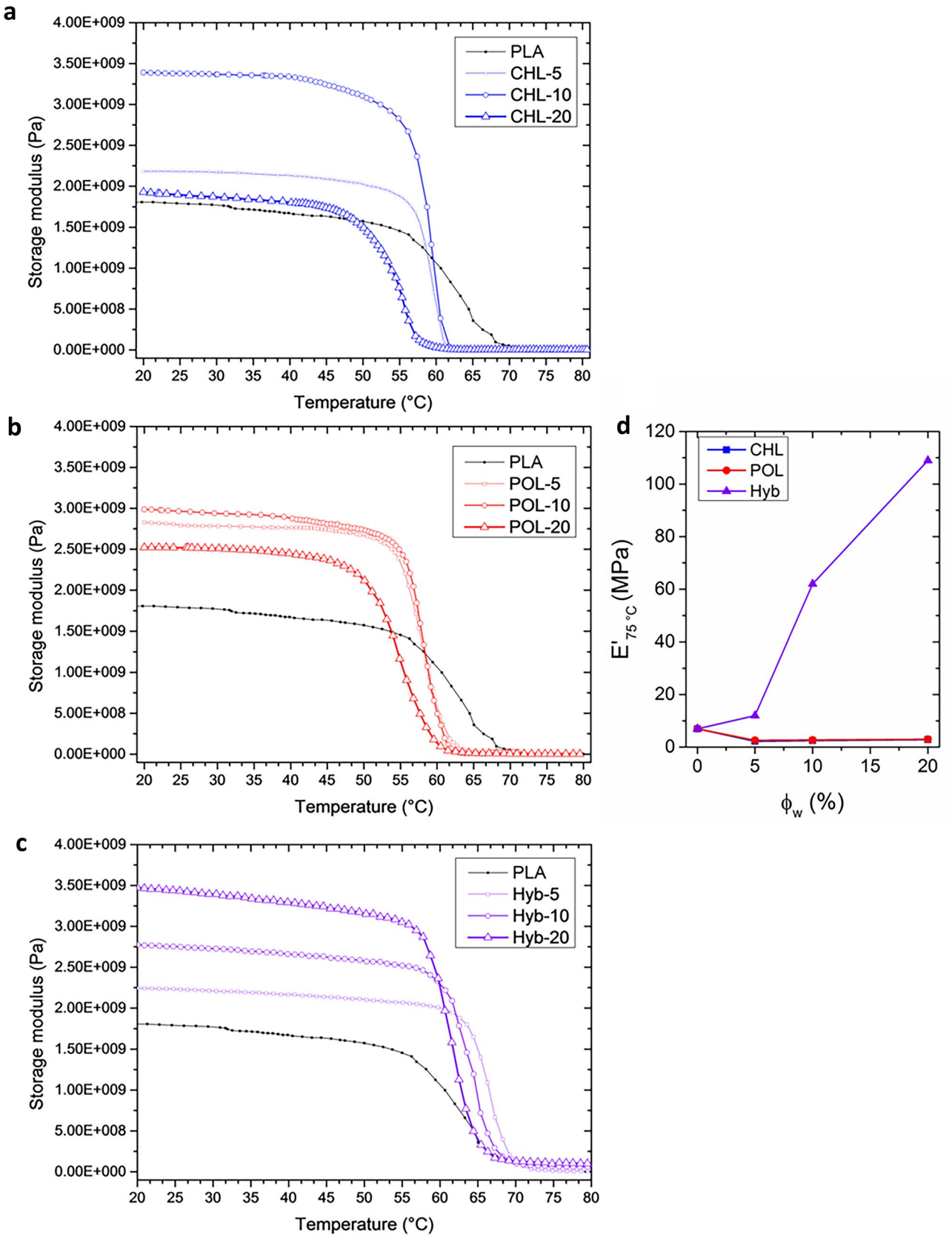

Fig. 8 E' plotted as a function of temperature for CHL-series (**a**), POL-series (**b**), and Hyb-series composites (**c**). E' at $T = 75$ °C plotted as a function of filler type and content (**d**)

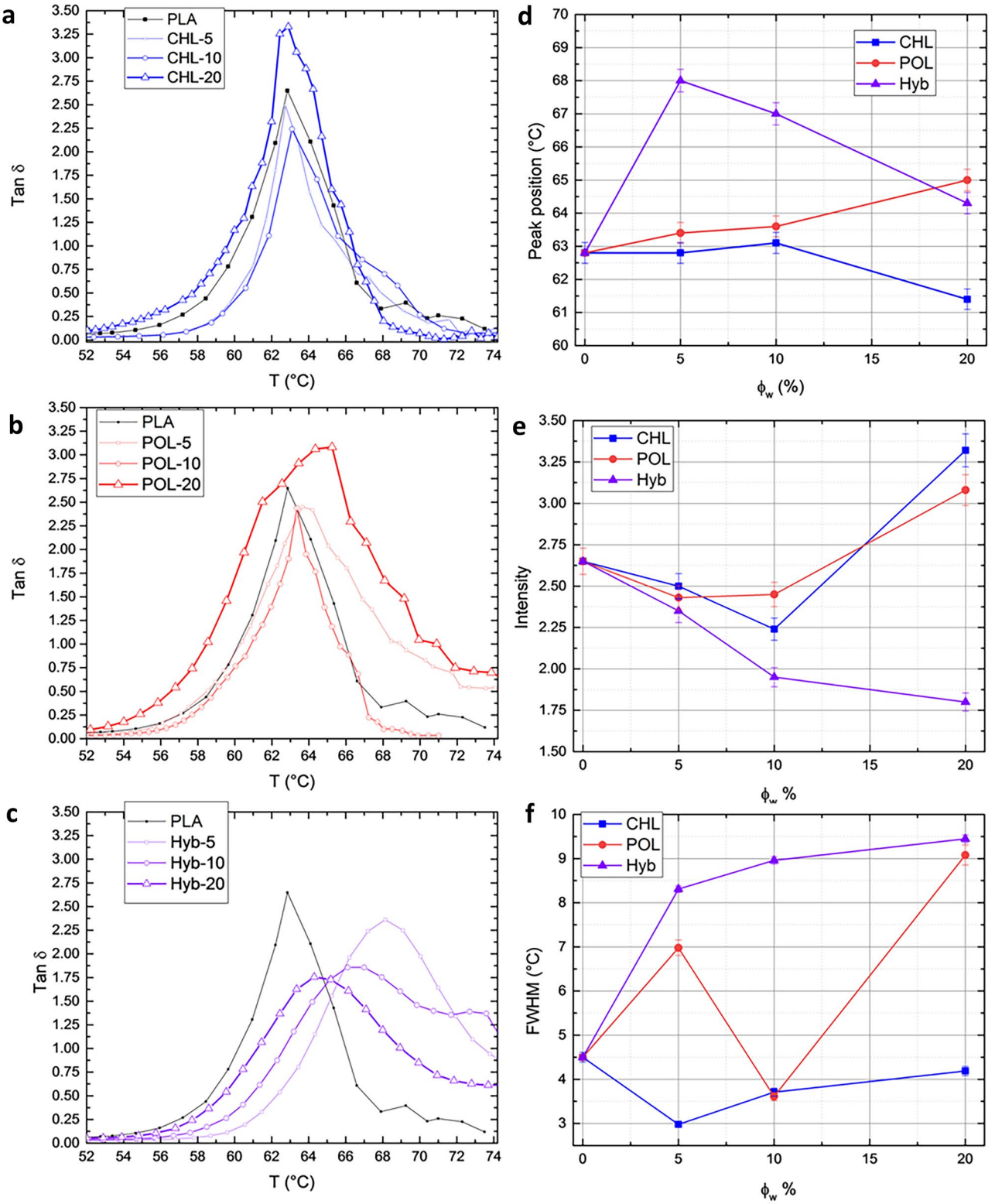

Fig. 9 Tan delta plotted as a function of temperature for CHL-series (**a**), POL-series (**b**), and Hyb-series composites (**c**). Peak position (**d**), intensity (**e**), and FWHM (**f**) of tan delta as a function of filler type and content

aspect could reasonably be ascribed to the balanced effects of geometrical features of hybrid network and fluidity of the polymer, which somehow resulted in the formation of a strong interphase.

Although in a microcomposite the quality and amount of interphase should play a less significant role with respect to the case of nanostructured systems, the materials herein investigated show porous fillers partially interpenetrated by polymer chains, with possible increase of filler-matrix interface. On the other hand, voids due to lack of adhesion or low dispersion degree would be detrimental. In this latter regard, DMA can provide useful information on the type of filler-matrix interactions [46]. Figure 8 reports storage moduli (E') of the CHL (a), POL (b), and Hyb (c) composites plotted as a function of temperature, along with the behavior of E' measured in the rubbery region ($T = 75$ °C), as a function of type and content of filler (d).

All the materials show a gradually declining storage modulus that eventually drops rapidly at a given temperature [47]. Notably, the E' values at room temperature are practically coincident with those of tensile tests. The differences observed among the samples in the way the curves drop in the rubbery region suggest that the extent and quality of interphase region play the main role. Indeed, in the rubbery region (Fig. 8d), all the biocomposites containing solely CHL or POL showed storage moduli lower than that of neat matrix, whereas hybrid biocomposites displayed values 10 times higher, thus exhibiting the best performance in the whole composition range investigated and an enhanced thermal stability [48]. Hence, the behavior of peak position, intensity, and FWHM of the damping band (tan delta) as a function of temperature was studied (Fig. 9). In fact, in a composite system, the presence of a filler affects the damping of polymeric chains, due to shear stress concentrations [49]. It is possible to correlate the changes in interfacial bonding to those in tan δ intensity: the higher the damping at the interfaces, the poorer the interface adhesion, since a composite with poor interface bonding tends to dissipate more energy than that with good interface bonding [50]. The width of tan δ band is indicative of the distribution of free and constrained amorphous phases, whereas eventual shifts in peak position could be ascribed to a lower or higher energy level required for the macromolecule motion and could be influenced by stress field surrounding the particles. Noteworthy, increased FWHM coupled with increased intensity and/or peak position downshift might indicate thermal degradation. The analysis of these data highlights that only hybrid composites experience a monotonic decrease of intensity accompanied by the progressive increase of FWHM as a function of filler content, thus suggesting that hybrid loading of CHL and POL led to the formation of a strong and extensive interphase region. Indeed, the trend of such features upon filler content is in strong agreement with the monotonic enhancement of TS and E observed during tensile tests, thus indicating that mechanical performance of hybrid biocomposites is governed by interphase. Moreover, Hyb-5 and Hyb-10 were the only composites that showed upshift in peak position if compared to neat PLA, whereas all the remaining samples displayed a downshift, likely indicative of competing phenomena, such as polymer degradation, low dispersion level, or scarce affinity between filler and matrix. Indeed, the plots of tan delta intensity in CHL- and POL-composites show positive concavity, with maxima at 20% filler for both systems, likely suggesting that after a certain concentration threshold any benefit is lost. The width of loss factor band in PLA/CHL composites proved to be lower than that of PLA, whereas PLA/POL composites show no clear trend with filler content. The former result can be likely ascribed to weak interfacial adhesion and low dispersion degree, while the latter reflects the above discussed complex relationship between matrix degradation and morphology.

4 Conclusion

Platelet-like and fibrous lignocellulosic fillers were obtained from the leaves of *Chamaerops humilis* (CHL) and *Posidonia oceanica* (POL) and successfully used as a hybrid reinforcement for a PLA matrix. When compared to their counterparts containing either CHL or POL only, the resulting hybrid biocomposites showed the highest mechanical and dynamic-mechanical properties, likely due to the formation of a strong and extensive interphase region, promoted by the balanced effect of morphological features of the hybrid network and physicochemical characteristics of the components. In detail, it was found that the elastic modulus and the tensile strength of PLA increase linearly with the hybrid filler content, with relative increments up to 88% and 22%, respectively. Otherwise, when CHL or POL is added individually, a general decay of breaking properties was observed, especially at high loading. A robust map of processing-structure-properties relationship was constructed by examining the behavior of some key morphological features of composites (i.e., densification, filler aspect ratio, and dispersion), two crucial physicochemical characteristics of the matrix, namely molecular weight and crystallinity, and the interphase region. The analysis pointed out that the overall best performance of hybrid biocomposites with respect to their counterparts is mainly governed by the formation of a strong and extensive interphase, prompted by the synergistic efficiency of the two fillers, which resulted in strengthening and stiffening effects respectively 120% and 30% higher than expected. The outcomes of this work provide further guidance for the design of robust and environmentally friendly materials from waste biosources.

Supplementary Information The online version contains supplementary material available at https://doi.org/10.1007/s42114-022-00534-y.

Funding Open access funding provided by Università degli Studi di Palermo within the CRUI-CARE Agreement.

Declarations

Conflict of interest The authors declare no competing interests.

References

1. Gu H, Gao C, Zhou X, Du A, Naik N, Guo Z (2021) Nanocellulose nanocomposite aerogel towards efficient oil and organic solvent adsorption. Adv Compos Hybrid Mater 4:459–468. https://doi.org/10.1007/s42114-021-00289-y
2. More AP (2022) Flax fiber–based polymer composites: a review. Adv Compos Hybrid Mater 5:1–20. https://doi.org/10.1007/s42114-021-00246-9
3. Ghosh S, Ghosh S, Pramanik N (2020) Bio-evaluation of doxorubicin (DOX)-incorporated hydroxyapatite (HAp)-chitosan (CS) nanocomposite triggered on osteosarcoma cells. Adv Compos Hybrid Mater 3:303–314. https://doi.org/10.1007/s42114-020-00154-4
4. Scaffaro R, Maio A, Gulino EF, Megna B (2019) Structure-property relationship of PLA-Opuntia ficus indica biocomposites. Compos B Eng 167:199–206. https://doi.org/10.1016/j.compositesb.2018.12.025
5. Scaffaro R, Maio A, Lopresti F (2018) Physical properties of green composites based on poly-lactic acid or Mater-Bi® filled with Posidonia oceanica leaves. Compos A Appl Sci Manuf 112:315–327. https://doi.org/10.1016/j.compositesa.2018.06.024
6. Scaffaro R, Maio A, Gulino EF, Alaimo G, Morreale M (2021) Green composites based on PLA and agricultural or marine waste prepared by FDM. Polymers (Basel) 13. https://doi.org/10.3390/polym13091361
7. Gunti R, Ratna Prasad AV, Gupta AV (2018) Mechanical and degradation properties of natural fiber-reinforced PLA composites: jute, sisal, and elephant grass. Polym Compos 39:1125–1136. https://doi.org/10.1002/pc.24041
8. Fu H, Xu H, Liu Y, Yang Z, Kormakov S, Wu D et al (2020) Overview of injection molding technology for processing polymers and their composites. ES Mater Manuf 8:3–23. https://doi.org/10.30919/esmm5f713
9. Naik V, Kumar M, Vijayan V, Kaup A (2022) A review on natural fiber composite material in automotive applications. Eng Sci 18:1–10. https://doi.org/10.30919/es8d589
10. Atta OM, Manan S, Ul-Islam M, Ahmed AA, Ullah MW, Yang G (2021) Silver decorated bacterial cellulose nanocomposites as antimicrobial food packaging materials. ES Food Agrofor 6:12–26. https://doi.org/10.30919/esfaf590
11. Shahabaz SM, Sharma S, Shetty N, Shetty SD, Gowrishankar MC (2021) Influence of temperature on mechanical properties and machining of fibre reinforced polymer composites: a review. Eng Sci 16:26–46. https://doi.org/10.30919/es8d553
12. Zhang D, Sun J, Lee LJ, Castro JM (2020) Overview of ultrasonic assisted manufacturing multifunctional carbon nanotube nanopaper based polymer nanocomposites. Eng Sci 10:35–50. https://doi.org/10.30919/es5e1002
13. Scaffaro R, Maio A, Re G Lo, Parisi A, Busacca A (2018) Advanced piezoresistive sensor achieved by amphiphilic nanointerfaces of graphene oxide and biodegradable polymer blends. Compos Sci Technol 156:166–176. https://doi.org/10.1016/j.compscitech.2018.01.008
14. Scaffaro R, Botta L, Maio A, Gallo G (2017) PLA graphene nanoplatelets nanocomposites: physical properties and release kinetics of an antimicrobial agent. Compos B Eng 109:139–146. https://doi.org/10.1016/j.compositesb.2016.10.058
15. Zhou Y, Wang P, Ruan G, Xu P, Ding Y (2021) Synergistic Effect of P [MPEGMA-IL] Modified graphene on morphology and dielectric properties of PLA/PCL blends. ES Mater Manuf 11:20–29. https://doi.org/10.30919/esmm5f928
16. Wang Y, Wang P, Du Z, Liu C, Shen C, Wang Y (2022) Electromagnetic interference shielding enhancement of poly(lactic acid)-based carbonaceous nanocomposites by poly(ethylene oxide)-assisted segregated structure: a comparative study of carbon nanotubes and graphene nanoplatelets. Adv Compos Hybrid Mater 5:209–219. https://doi.org/10.1007/s42114-021-00320-2
17. Scaffaro R, Gulino EF, Citarrella MC, Maio A (2022) Green composites based on Hedysarum coronarium with outstanding FDM printability and mechanical performance. Polymers (Basel) 14. https://doi.org/10.3390/polym14061198
18. Scaffaro R, Maio A (2019) Integrated ternary bionanocomposites with superior mechanical performance via the synergistic role of graphene and plasma treated carbon nanotubes. Compos B Eng. https://doi.org/10.1016/j.compositesb.2019.03.076
19. Asaithambi B, Ganesan G, Ananda KS (2014) Bio-composites: development and mechanical characterization of banana/sisal fibre reinforced poly lactic acid (PLA) hybrid composites. Fibers Polym 15:847–854. https://doi.org/10.1007/s12221-014-0847-y
20. Angin N, Caylak S, Ertas M, Cavdar AD (2022) Effect of alkyl ketene dimer on chemical and thermal properties of polylactic acid (PLA) hybrid composites. Sustain Mater Technol e00386. https://doi.org/10.1016/j.susmat.2021.e00386
21. Vinod A, Gowda Y, Krishnasamy S, Sanjay MR, Siengchin S (2022) Natural Fiber-Reinforced Composites: Thermal Properties and Applications. John Wiley & Sons Ltd, pp 17–30. https://doi.org/10.1002/9783527831562.ch2
22. Liu H, Gao J, Huang W, Dai K, Zheng G, Liu C et al (2016) Electrically conductive strain sensing polyurethane nanocomposites with synergistic carbon nanotubes and graphene bifillers. Nanoscale 8:12977–12989. https://doi.org/10.1039/c6nr02216b
23. Zhang J-X, Liang Y-X, Wang X, Zhou H-J, Li S-Y, Zhang J et al (2018) Strengthened epoxy resin with hyperbranched polyamine-ester anchored graphene oxide via novel phase transfer approach. Adv Compos Hybrid Mater 1:300–309. https://doi.org/10.1007/s42114-017-0007-0
24. Zhang J, Zhang W, Wei L, Pu L, Liu J, Liu H et al (2019) Alternating multilayer structural epoxy composite coating for corrosion protection of steel. Macromol Mater Eng 304:1900374. https://doi.org/10.1002/mame.201900374
25. Liu J, Zhang J, Tang J, Pu L, Xue Y, Lu M et al (2020) Polydimethylsiloxane resin nanocomposite coating with alternating multilayer structure for corrosion protection performance. ES Mater Manuf 10:29–38. https://doi.org/10.30919/esmm5f912
26. Li S, Yang P, Liu X, Zhang J, Xie W, Wang C et al (2019) Graphene oxide based dopamine mussel-like cross-linked

polyethylene imine nanocomposite coating with enhanced hexavalent uranium adsorption. J Mater Chem A 7:16902–16911. https://doi.org/10.1039/C9TA04562G
27. Li Y, Zhang T, Jiang B, Zhao L, Liu H, Zhang J et al (2019) Interfacially reinforced carbon fiber silicone resin via constructing functional nano-structural silver. Compos Sci Technol 181:107689. https://doi.org/10.1016/j.compscitech.2019.107689
28. Guo Y, Yang X, Ruan K, Kong J, Dong M, Zhang J et al (2019) Reduced graphene oxide heterostructured silver nanoparticles significantly enhanced thermal conductivities in hot-pressed electrospun polyimide nanocomposites. ACS Appl Mater Interfaces 11:25465–25473. https://doi.org/10.1021/acsami.9b10161
29. Wang Y, Jiang D, Zhang L, Li B, Sun C, Yan H et al (2019) Hydrogen bonding derived self-healing polymer composites reinforced with amidation carbon fibers. Nanotechnology 31:25704. https://doi.org/10.1088/1361-6528/ab4743
30. Qian Y, Yuan Y, Wang H, Liu H, Zhang J, Shi S et al (2018) Highly efficient uranium adsorption by salicylaldoxime/polydopamine graphene oxide nanocomposites. J Mater Chem A 6:24676–24685. https://doi.org/10.1039/C8TA09486A
31. Stephen C, Shivamurthy B, Mohan M, Mourad AH, Selvam R, Thimmappa BH (2022) Low Velocity Impact Behavior of Fabric Reinforced Polymer Composites–A Review. Eng Sci 18:75–97. https://doi.org/10.30919/es8d670
32. de Macedo Neto JC, do Nascimento NR, Bello RH, de Verçosa LA, Neto JE, da Costa JC et al (2022) Kaolinite review: intercalation and production of polymer nanocomposites. Eng Sci 17:28–44. https://doi.org/10.30919/es8d499
33. Chen J, Zhu Y, Guo Z, Nasibulin AG (2020) Recent progress on thermo-electrical properties of conductive polymer composites and their application in temperature sensors. Eng Sci 12:13–22. https://doi.org/10.30919/es8d1129
34. Zhang Z, Zhang J, Li S, Liu J, Dong M, Li Y et al (2019) Effect of graphene liquid crystal on dielectric properties of polydimethylsiloxane nanocomposites. Compos B Eng 176:107338. https://doi.org/10.1016/j.compositesb.2019.107338
35. Gao Y, Zhang J, Zhang Z, Li Z, Xiong Q, Deng L et al (2021) Plasmon-enhanced perovskite solar cells with efficiency beyond 21 %: the asynchronous synergistic effect of water and gold nanorods. ChemPlusChem 86:291–297. https://doi.org/10.1002/cplu.202000792
36. Scaffaro R, Gammino M, Maio A (2022) Wet electrospinning-aided self-assembly of multifunctional GO-CNT@PCL core-shell nanocomposites with spider leg bioinspired hierarchical architectures. Compos Sci Technol 221:109363. https://doi.org/10.1016/j.compscitech.2022.109363
37. Scaffaro R, Maio A, Gulino EF, Pitarresi G (2020) Lignocellulosic fillers and graphene nanoplatelets as hybrid reinforcement for polylactic acid: effect on mechanical properties and degradability. Compos Sci Technol 190. https://doi.org/10.1016/j.compscitech.2020.108008
38. Scaffaro R, Maio A, Gulino EF (2021) Hydrolytic degradation of PLA/Posidonia oceanica green composites: a simple model based on starting morpho-chemical properties. Compos Sci Technol 213:108930. https://doi.org/10.1016/j.compscitech.2021.108930
39. Scaffaro R, Maio A, Gammino M, Alaimo G (2022) Modelling the structure-property relationships of high performance PBAT-based biocomposites with natural fibers obtained from Chamaerops humilis dwarf palm. Compos Sci Technol 223:109427. https://doi.org/10.1016/j.compscitech.2022.109427
40. Du Y, Wu T, Yan N, Kortschot MT, Farnood R (2014) Fabrication and characterization of fully biodegradable natural fiber-reinforced poly(lactic acid) composites. Compos B Eng 56:717–723. https://doi.org/10.1016/j.compositesb.2013.09.012
41. Morreale M, Scaffaro R, Maio A, La MFP (2008) Effect of adding wood flour to the physical properties of a biodegradable polymer. Compos A Appl Sci Manuf 39:503–513. https://doi.org/10.1016/j.compositesa.2007.12.002
42. Kalyon DM, Lawal A, Yazici R, Yaras P, Railkar S (1999) Mathematical modeling and experimental studies of twin-screw extrusion of filled polymers. Polym Eng Sci 39:1139–1151. https://doi.org/10.1002/pen.11501
43. Gong S, Cui W, Zhang Q, Cao A, Jiang L, Cheng Q (2015) Integrated ternary bioinspired nanocomposites via synergistic toughening of reduced graphene oxide and double-walled carbon nanotubes. ACS Nano 9:11568–11573. https://doi.org/10.1021/acsnano.5b05252
44. Chang X, Chen L, Chen J, Zhu Y, Guo Z (2021) Advances in transparent and stretchable strain sensors. Adv Compos Hybrid Mater 4:435–450. https://doi.org/10.1007/s42114-021-00292-3
45. Jing X, Li Y, Zhu J, Chang L, Maganti S, Naik N et al (2022) Improving thermal conductivity of polyethylene/polypropylene by styrene-ethylene-propylene-styrene wrapping hexagonal boron nitride at the phase interface. Adv Compos Hybrid Mater. https://doi.org/10.1007/s42114-022-00438-x
46. Bashir MA (2021) Use of dynamic mechanical analysis (DMA) for characterizing interfacial interactions in filled polymers. Solids 2:108–120. https://doi.org/10.3390/solids2010006
47. Seibert JR, Keleş Ö, Wang J, Erogbogbo F (2019) Infusion of graphene quantum dots to modulate thermal conductivity and dynamic mechanical properties of polymers. Polymer (Guildf) 185:121988. https://doi.org/10.1016/j.polymer.2019.121988
48. Ma P-C, Mo S-Y, Tang B-Z, Kim J-K (2010) Dispersion, interfacial interaction and re-agglomeration of functionalized carbon nanotubes in epoxy composites. Carbon N Y 48:1824–1834. https://doi.org/10.1016/j.carbon.2010.01.028
49. Maio A, Fucarino R, Khatibi R, Rosselli S, Bruno M, Scaffaro R (2015) A novel approach to prevent graphene oxide re-aggregation during the melt compounding with polymers. Compos Sci Technol 119. https://doi.org/10.1016/j.compscitech.2015.10.006
50. Scaffaro R, Maio A (2017) A green method to prepare nanosilica modified graphene oxide to inhibit nanoparticles re-aggregation during melt processing. Chem Eng J 308:1034–1047. https://doi.org/10.1016/j.cej.2016.09.131